Expansion Techniques in Massive Quark Production: Results and Applications

J.H. Kühn
Institut für Theoretische Teilchenphysik,
Universität Karlsruhe, D–76128 Karlsruhe, Germany

Recent progress in the calculation of multi-loop, multi-scale diagrams is reviewed. Expansion techniques combined with new developments in Computer algebra allow to evaluate the R ratio for massive quarks up to order α_s^2 and, partly, even α_s^3. Similar techniques can be applied to Higgs- or Z-boson decays and mixed QCD and electroweak interactions.

1 Introduction

During the past years amazing progress has been made in the experimental tests of the Standard Model of particle physics. Its electroweak sector has been scrutinized at LEP, mainly in Z decays and W pair production, and at the TEVATRON, mainly through the precise measurements of the W boson and top quark masses. Perturbative QCD has been tested at electron positron colliders at lower energies as well as in high energy experiments at LEP, at the TEVATRON through proton-antiproton collisions, and through lepton-nucleon scattering in particular at HERA.

The large statistics collected in these experiments in conjunction with the small systematic uncertainty allows to test the theoretical predictions with high precision, requiring the inclusion of quantum corrections at least in one-loop approximation, occasionally two or even three-loop calculations are required. This applies on one hand to perturbative QCD, for electroweak observables on the other hand either purely weak two-loop corrections should be included or so-called "mixed" QCD and electroweak effects up to two or even three loops. Considerable progress has been made on the theoretical side which matches these requirements. Two-loop amplitudes, in particular those contributing to two-point functions can often be evaluated in closed form or through straightforward numerical integrals — even with arbitrary mass assignments. Three-loop amplitudes, however, are at present only accessible in a few selected cases. These are, most notably, two-point functions with massless internal propagators only and vacuum diagrams with massless and massive propagators — however, of identical mass throughout. Other cases of interest are "on-shell amplitudes" required for mass renormalization and certain types of integrals relevant for fermion pair production at threshold.

Despite this seemingly limited set of diagrams a large variety of problems can be solved with the help of expansion techniques. Frequently one finds a hierarchy of mass and/or energy scales which suggests to perform a Taylor series of the integrand, with the resulting integrals being considerably simpler. However, the integrals are not necessarily analytic in the expansion parameter, and more refined techniques, denoted hard mass, large momentum [1,2] or threshold expansion [3,4,5] are required. These can be formulated in a diagrammatic manner and allow to reduce a given amplitude into an (infinite) sum of products of simpler "master" amplitudes which are known in analytical form. In practice often the first few terms provide already a sufficiently accurate numerical answer. In this approach, the demands on computation grow rapidly. Not only the Dirac algebra and the evaluation of integrals for individual diagrams has to be performed by computer algebra, with the appearance of hundreds if not thousands of diagrams also the generation of the basic diagrams, the application of the hard mass or large momentum procedure, the transformation of diagrams into algebraic expressions and the overall book keeping has to be performed automatically. (For a recent review see [6].)

In the following talk several characteristic examples will be given, partly taken from QCD, partly from electroweak interactions. The next chapter will be concerned with the $\mathcal{O}(\alpha_s^2)$ evaluation of the cross section for electron positron annihilation into massive quarks. Information on the vacuum polarization function at small and large $q^2/(4m^2)$ as obtained via expansion techniques is combined with the two dominant terms close to threshold. Subsequently a variable transformation is applied as suggested by the analyticity structure of $\Pi(q^2)$ in the cut complex plane. The numerical results will be contrasted with those deduced from the threshold expansion. Techniques, results and limitations of the large momentum procedure will be presented in chapter 3. This includes in particular the calculation of the vacuum polarization of order α_s^2, expanded in m^2/q^2 up to fairly high power. The strategy for an evaluation of the absorptive part in order $\alpha_s^3 m^2/q^2$ and $\alpha_s^3(m^2/q^2)^2$ and recent results are given in chapter 4. Results of relevance for electroweak measurements are discussed in chapter 5. This includes the top quark contribution to the ρ parameter in three-loop approximation, mixed corrections to the Z decay rate and "theory driven" results for the running QED coupling at scale M_Z. Chapter 6 contains a brief summary and the conclusions.

2 Three-Loop Heavy-Quark Vacuum Polarization

The measurement of the total cross section for electron positron annihilation into hadrons allows for a unique test of perturbative QCD. The decay rate $\Gamma(Z \to \text{hadrons})$ provides one of the most precise determinations of the strong coupling constant α_s. In the high energy limit the quark masses can often be neglected. In this approximation QCD corrections to $R \equiv \sigma(e^+e^- \to \text{hadrons})/\sigma(e^+e^- \to \mu^+\mu^-)$ have been calculated [7,8] up to order α_s^3. For precision measurements the dominant mass corrections must be included through an expansion in m^2/s. Terms up to order $\alpha_s^3 m^2/s$ (see [9]) and $\alpha_s^2 m^4/s^2$ (see [10]) and recently [11] even up to $\alpha_s^3 m^4/s^2$ are available at present, providing an acceptable approximation from the high energy region down to intermediate energy values. For a number of measurements, however, the information on the complete mass dependence is desirable. This includes charm and bottom meson production above the resonance region, say above 4.5 GeV and 12 GeV, respectively, and, of course, top quark production at a future electron positron collider. To order α_s this calculation was performed by Källén and Sabry in the context of QED a long time ago [12]. With measurements of ever increasing precision, predictions in order α_s^2 are needed for a reliable comparison between theory and experiment. Furthermore, when one tries to apply the $\mathcal{O}(\alpha)$ result to QCD, with its running coupling constant, the choice of scale becomes important. In fact, the distinction between the two intrinsically different scales, the relative momentum versus the center of mass energy, is crucial for a stable numerical prediction. This information can be obtained from a full calculation to order α_s^2 only. Such a calculation then allows to predict the cross section in the complete energy region where perturbative QCD can be applied — from close to threshold up to high energies. It is then only the region very close to threshold, where the fixed order result remains inadequate and Coulomb resummation becomes important. In [13] results for the cross section were calculated in order α_s^2. They were obtained from the vacuum polarization $\Pi(q^2)$ which was calculated up to three loops. The imaginary part of the "fermionic contribution" — derived from diagrams with a massless quark loop inserted in the gluon propagator — had been calculated earlier in [14]. In this latter case all integrals could be performed to the end and the result was expressed in terms of polylogarithms. In [13] the calculation was extended to the full set of diagrams relevant for QCD. Instead of trying to perform the integrals analytically, information of $\Pi(q^2)$ from the large q^2 behaviour, the expansion around $q^2 = 0$ and from threshold was incorporated.

2.1 Outline of the Calculation [13]

The different behaviour at threshold makes it necessary to decompose Π according to its colour structure. It is convenient to write:

$$\Pi(q^2) = \Pi^{(0)}(q^2) + \frac{\alpha_s(\mu^2)}{\pi} C_F \Pi^{(1)}(q^2) + \left(\frac{\alpha_s(\mu^2)}{\pi}\right)^2 \Pi^{(2)}(q^2) + \cdots, \quad (1)$$

$$\Pi^{(2)} = C_F^2 \Pi_A^{(2)} + C_A C_F \Pi_{NA}^{(2)} + C_F T n_l \Pi_l^{(2)} + C_F T \Pi_F^{(2)}. \tag{2}$$

The same notation is adopted to the physical observable $R(s)$ which is related to $\Pi(q^2)$ by

$$R(s) = 12\pi \,\mathrm{Im}\Pi(q^2 = s + i\epsilon). \tag{3}$$

The contributions from diagrams with n_l light or one massive internal fermion loop are denoted by $C_F T n_l \Pi_l^{(2)}$ and $C_F T \Pi_F^{(2)}$, respectively. The purely gluonic corrections are proportional to C_F^2 or $C_A C_F$ where the former are the only contributions in an Abelian theory and the latter are characteristic for the non-Abelian aspects of QCD.

All steps described below have been performed separately for the first three contributions to $\Pi^{(2)}$. In fact, new information is only obtained for $\Pi_A^{(2)}$ and $\Pi_{NA}^{(2)}$ since $\mathrm{Im}\Pi_l^{(2)}$ is already known analytically [14]. The contribution from a four-particle cut with threshold at $4m$ is given in terms of a two dimensional integral [14,15] which can be solved easily numerically, so $\Pi_F^{(2)}$ will not be treated.

Let us now discuss the behaviour of $\Pi(q^2)$ in the three different kinematical regions and the approximation method.

Analysis of the high q^2 behaviour: The high energy behaviour of Π provides important constraints on the complete answer. In the limit of small m^2/q^2 the constant term and the one proportional to m^2/q^2 (modulated by powers of $\ln(\mu^2/q^2)$ have been calculated a long time ago [16]. The results for terms up to order $(m^2/q^2)^4$ are described in chapter 3, provide an important cross check, however, they are not used for the moment.

Threshold behaviour: General arguments based on the influence of Coulomb exchange close to threshold, combined with the information on the perturbative QCD potential and the running of α_s dictate the singularities and the structure of the leading cuts close to threshold, that is for small $v = \sqrt{1 - 4m^2/s}$. The C_F^2 term is directly related to the QED result with internal photon lines only. The leading $1/v$ singularity and the constant term of R_A can be predicted from the nonrelativistic Greens function for the Coulomb potential and the $\mathcal{O}(\alpha_s)$ calculation. The next-to-leading term is determined by the combination of one-loop results again with the Coulomb singularities [17]. One finds

$$R_A^{(2)} = 3\left(\frac{\pi^4}{8v} - 3\pi^2 + \ldots\right). \tag{4}$$

The contributions $\sim C_A C_F$ and $\sim C_F T n_l$ can be treated in parallel. For these colour structures the perturbative QCD potential [18]

$$V_{\mathrm{QCD}}(\vec{q}^{\,2}) = -4\pi C_F \frac{\alpha_V(\vec{q}^{\,2})}{\vec{q}^{\,2}}, \tag{5}$$

$$\alpha_V(\vec{q}^{\,2}) = \alpha_s(\mu^2)\left[1 + \frac{\alpha_s(\mu^2)}{4\pi}\left(\left(\frac{11}{3}C_A - \frac{4}{3}Tn_l\right)\left(-\ln\frac{\vec{q}^{\,2}}{\mu^2} + \frac{5}{3}\right) - \frac{8}{3}C_A\right)\right]$$

will become important. The leading C_AC_F and C_FTn_l term in R is proportional to $\ln v$ and is responsible for the evolution of the coupling constant close to threshold. Also the constant term can be predicted by the observation, that the leading term in order α_s is induced by the potential. The $\mathcal{O}(\alpha_s)$ result

$$R = 3\frac{v(3-v^2)}{2}\left(1 + C_F\frac{\pi^2(1+v^2)}{2v}\frac{\alpha_s}{\pi} + \ldots\right) \tag{6}$$

is employed to predict the logarithmic and constant C_FC_A and C_FTn_l terms of $\mathcal{O}(\alpha_s^2)$ by replacing α_s by $\alpha_V(4\vec{p}^{\,2} = v^2 s)$ as given in Eq. (6). This implies the following threshold behaviour:

$$R_{NA}^{(2)} = 3\frac{\pi^2}{3}(3-v^2)(1+v^2)\left(-\frac{11}{16}\ln\frac{v^2 s}{\mu^2} + \frac{31}{48} + \ldots\right), \tag{7}$$

$$R_l^{(2)} = 3\frac{\pi^2}{3}(3-v^2)(1+v^2)\left(\frac{1}{4}\ln\frac{v^2 s}{\mu^2} - \frac{5}{12} + \ldots\right). \tag{8}$$

This ansatz suggested in [13] can be verified for the C_FTn_l term where the result is known in analytical form [14] and it has also been confirmed for the NA term where the leading terms for small v have been derived recently (see below). Extending the ansatz from the behaviour of the imaginary part close to the branching point into the complex plane allows to predict the leading terms of $\Pi(q^2) \sim \ln v$ and $\sim \ln^2 v$.

Behaviour at $q^2 = 0$: Important information is contained in the Taylor series of $\Pi(q^2)$ around zero. The calculation of the first seven nontrivial terms is based on the evaluation of three-loop tadpole integrals with the help of the algebraic program `MATAD` written in `FORM` [19] which performs the traces, calculates the derivatives with respect to the external momenta. It reduces the large number of different integrals to one master integral and a few simple ones through an elaborate set of recursion relations based on the integration-by-parts method [20,21]. The result can be written in the form:

$$\Pi^{(2)} = \frac{3}{16\pi^2}\sum_{n>0} C_n^{(2)}\left(\frac{q^2}{4m^2}\right)^n, \tag{9}$$

where the first seven moments are listed in [13].

Conformal mapping and Padé approximation: The vacuum polarization function $\Pi^{(2)}$ is analytic in the complex plane cut from $q^2 = 4m^2$ to $+\infty$. The

Taylor series in q^2 is thus convergent in the domain $|q^2| < 4m^2$ only. The conformal mapping which corresponds to the variable transformation ($z = q^2/(4m^2)$)

$$\omega = \frac{1-\sqrt{1-z}}{1+\sqrt{1-z}}, \qquad z = \frac{4\omega}{(1+\omega)^2}, \tag{10}$$

transforms the cut complex z plane into the interior of the unit circle. The special points $z = 0, 1, -\infty$ correspond to $\omega = 0, 1, -1$, respectively (Fig. 1).

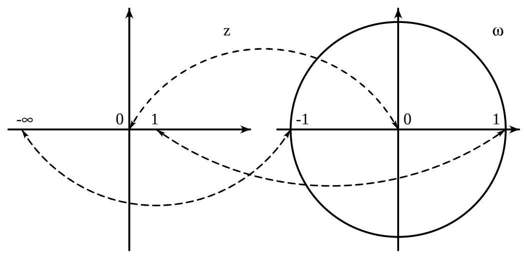

Figure 1: Transformation between the z and ω plane

The upper (lower) part of the cut is mapped onto the upper (lower) perimeter of the circle. The Taylor series in ω thus converges in the interior of the unit circle. To obtain predictions for $\Pi(q^2)$ at the boundary it has been suggested [22,23] to use the Padé approximation which converges towards $\Pi(q^2)$ even on the perimeter. To improve the accuracy the singular threshold behaviour and the large q^2 behaviour is incorporated into simple analytical functions which are removed from $\Pi^{(2)}$ before the Padé approximation is performed. The quality of this procedure can be tested by comparing the prediction with the known result for $\mathrm{Im}\Pi_l^{(2)}$.

The logarithmic singularities at threshold and large q^2 are removed by subtraction, the $1/v$ singularity, which is present for the C_F^2 terms only, by multiplication with v as suggested in [24]. The imaginary part of the remainder which is actually approximated by the Padé method is thus smooth in the entire circle, numerically small and vanishes at $\omega = 1$ and $\omega = -1$.

2.2 Results

After performing the Padé approximation for the smooth remainder with ω as natural variable, the transformation (10) is inverted and the full vacuum polarization function reconstructed by reintroducing the threshold and high energy

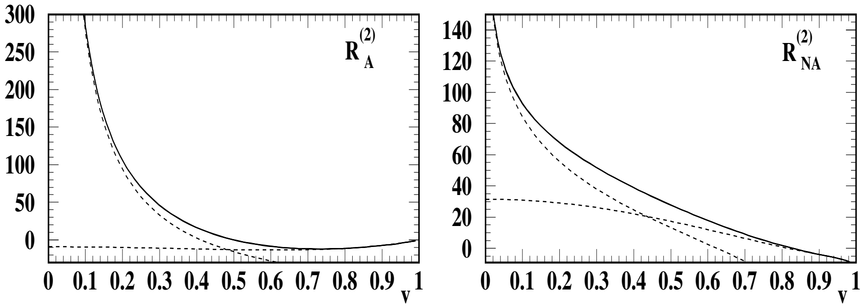

Figure 2: Complete results (full line) are compared to the threshold approximations and the high energy approximations including the m^2/s (dash-dotted) and the m^4/s^2 (dashed) terms ($x = 2m/\sqrt{s}$).

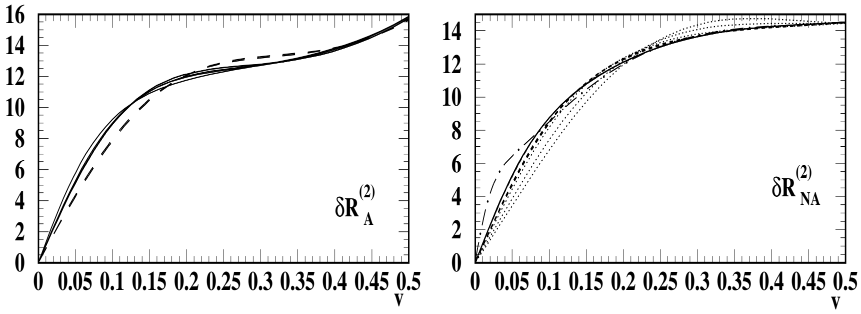

Figure 3: The threshold behaviour of the remainder δR for three different Padé approximants is shown. (The singular and constant parts around threshold are subtracted.)

terms. This procedure provides real and imaginary parts of $\Pi^{(2)}$. Subsequently only the absorptive part of $\Pi^{(2)}$ (multiplied by 12π) will be presented.

In the following it will be useful to plot the results as functions of $x = 2m/\sqrt{s}$ and alternatively of $v = \sqrt{1 - 4m^2/s}$. The first choice is particularly useful for investigations of the high energy region, the second one for energies close to threshold. Characteristic values of x, v and $\sqrt{s}$ for charm (m_c = 1.6 GeV), bottom (m_b = 4.7 GeV) and top (m_t = 175 GeV) quarks are listed in Table 1 for easy comparisons. Energy values where a perturbative treatment is evidently inapplicable are denoted by dashes.

In Fig. 2 the complete results are shown for $\mu^2 = m^2$ with $R_A^{(2)}$ and $R_{NA}^{(2)}$ displayed separately. The solid line represents the full correction. The threshold approximation is given by the dashed curve. In the high energy region

x	0.1	0.2	0.3	0.4	0.5	0.6	0.7	0.8	0.9	0.95	0.97	0.98
v	0.995	0.980	0.954	0.917	0.866	0.800	0.714	0.600	0.436	0.312	0.243	0.199
$\sqrt{s_c}$	32	16	10.7	8.0	6.4	5.3	4.6	4.0	—	—	—	—
$\sqrt{s_b}$	94	47	31.3	23.5	18.8	15.7	13.4	11.8	10.4	—	—	—
$\sqrt{s_t}$	3500	1750	1167	875	700	583	500	438	389	368	361	357

Table 1: Conversion between x and v and values for $\sqrt{s}$ in GeV for charm, bottom and top production.

the corrections containing the m^2/s terms and the quartic approximations are included. It should be stressed that the latter are not incorporated into the construction of $R^{(2)}$ but they are evidently very well reproduced by the method presented here. This will be investigated in more detail in chapter 3. There it will be demonstrated that the high energy expansion (including sufficiently many terms) and the Padé result agree remarkably well between $x = 0$ and $x = 0.7$ which covers most of the perturbative region for charmed and bottom quarks.

The results which include high moments up to C_6, C_7 or even C_8 are remarkably stable down to very small values of v. Different Padé approximations of the same degree and approximants with a reduced number of parameters give rise to practically identical predictions, which could hardly be distinguished in Fig. 2. Minor variations are observed close to threshold, *after* subtracting the singular and constant parts. The remainder δR for up to ten different Padé approximants is shown in Fig. 3. In [13] it was demonstrated that there is a perfect agreement for $R_l^{(2)}$; $R_{NA}^{(2)}$ seems to converge to the solid line ($[4/4], [5/3]$ and $[3/5]$) when more moments from small q^2 are included. The dashed lines are from the $[3/3], [4/2], [2/4]$ and $[3/4]$, the dotted ones from lower order Padé approximants. The dash-dotted curve is the $[4/3]$ Padé approximant and has a pole very close to $\omega = 1(1.07\ldots)$. For the Abelian part a classification of the different results can be seen: the dashed lines are $[4/2]$ and $[2/4]$, the solid ones $[3/2], [2/3], [5/3], [3/5]$ and $[5/4]$ Padé approximants.

Recently additional terms from the high energy expansion have been injected in the Padé approximation [11,25]. The results, shown in Fig. 4 confirm those from [13] and demonstrate the stability of the Padé approximation. It must be stressed that a safe estimate of the remaining uncertainty in R_A and R_{NA} amounts to less than 0.02 for v above 0.1 and is around 0.05 in the region $v \approx 0.03$. This region is, however, entirely dominated by the singular and constant terms with values around 50 and higher. The perturbative predictions for R are therefore under excellent control. It goes without saying that the function $\Pi(q^2)$ constructed this way and evaluated e.g. in the Euclidean region

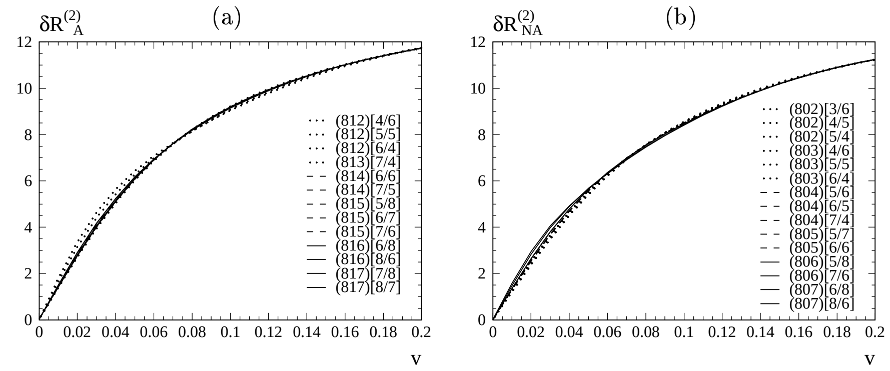

Figure 4: Variation of the prediction for $R_A^{(2)}$ and $R_{NA}^{(2)}$ by including an increasing number of terms from the high energy expansion. The singular and constant pieces at $v = 0$ have been subtracted. (From [11].)

could be a useful tool for other investigations of interest, for example for sum rules involving massive quarks.

Quite some effort has been invested in the analytic evaluation of R_A and R_{NA} close to threshold. As stated above, the singular and constant terms (Eqs. (4), (7) and (8)) were derived through general considerations [17,13]. To evaluate the $v \ln v$ and the v terms, however, elaborate analytical calculations of the two-loop form factor were used [26,4] with the results

$$
\begin{aligned}
R_A = 3\Bigg\{ & \frac{\pi^4}{8v} - 3\,\pi^2 + v\,\Bigg(-\frac{\pi^4}{24} \\
& + \frac{3}{2}\,(\frac{\pi^4}{6} + \pi^2\,(-\frac{35}{18} - \frac{2}{3}\,\ln v + \frac{4}{3}\,\ln 2) + \frac{39}{4} - \zeta(3))\Bigg)\Bigg\} \qquad (11) \\
R_{NA} = 3\Bigg\{ & \pi^2\,\left(\frac{31}{48} - \frac{11}{8}\,\ln 2v\right) \\
& + \frac{3}{2}\,v\,\left(\pi^2\,(\frac{179}{72} - \ln v - \frac{8}{3}\,\ln 2) - \frac{151}{36} - \frac{13}{2}\,\zeta(3)\right)\Bigg\} \qquad (12)
\end{aligned}
$$

While the result for R_A was still obtained in the framework of "classical" QED calculations, R_{NA} was calculated using a convenient technique which formalized the expansion for small v (see [3,4,5]). Padé and small v results are compared in Fig. 6, again subtracting first the singular and constant pieces. The slopes for very small v predicted by the two approaches are again in nice agreement, giving further credibility to the Padé result. However, it is also

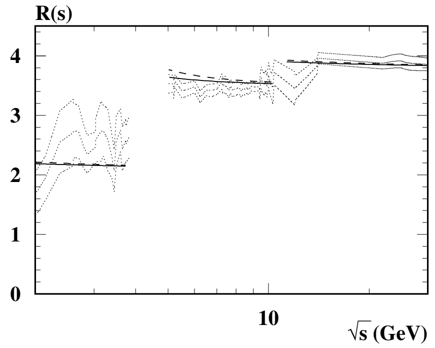

Figure 5: $R(s)$ plotted against $\sqrt{s}$. The scale $\mu^2 = s$ has been adopted. The dashed curves correspond to the values $M_c = 1.8$ GeV, $M_b = 5.0$ GeV and $\alpha_s(M_Z^2) = 0.121$, whereas for the solid curves $M_c = 1.4$ GeV, $M_b = 4.4$ GeV and $\alpha_s(M_Z^2) = 0.115$ is used. The dotted lines show a recent compilation of the available experimental data. The central curves correspond to the mean values, upper and lower curves indicate the combined statistical and systematical errors. (From [15].)

clear from this comparison that the small v expansion alone cannot lead to a reliable prediction over a larger energy range. This is explicitely demonstrated for the case of R_l where the analytic result is available. Terms at least of order v^3 are needed for a stable prediction.

A compilation of theoretical results can be found in [15] where the prediction for massive quark production is compared with the measurements over a wide energy region (Fig. 5).

Up to this point only the vector current correlator has been discussed. However, the techniques described above have also been applied to other currents [27]: the axial vector, relevant e.g. for top production through the virtual Z boson, as well as scalar and pseudoscalar currents describing for example the decay of Higgs bosons into massive quarks. Recently also the singlet piece of top quark production through the axial current was evaluated [28], completing thus the $\mathcal{O}(\alpha_s^2)$ prediction of massive quark production.

3 Large Momentum Expansions

An alternative route towards an efficient evaluation of the polarization function is based on the large momentum expansion. In this case the polarization function $\Pi(q^2)$ is expanded in powers of m^2/q^2, multiplied by logarithms of m^2/q^2, with the power of the logarithms, however, limited by the number of

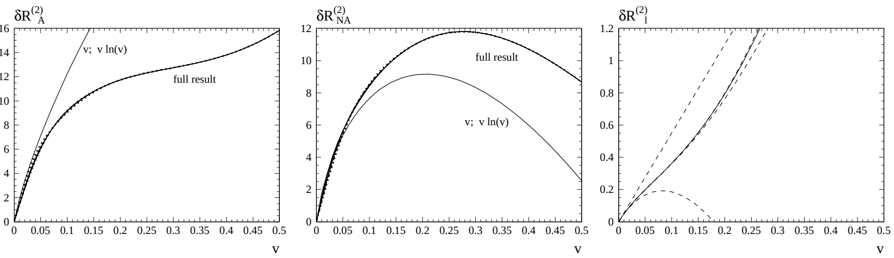

Figure 6: Comparison of the small v expansion (solid curves) of δR_A, δR_{NA} with the full result (solid and dotted curves) after subtraction of the singular and constant pieces. The difference between dotted and solid curve indicate the remaining uncertainty of the semianalytical result. For δR_l successive approximations of the small v expansion (dashed curves) and exact result (solid) are shown.

loops under consideration. Technically the expansion is given by a series of products of massless propagator and massive tadpole integrals.

In principle the full information on the analytic function is contained in this series. The structure of the integrals is simplified by moving from two- to one-scale integrals. However, an enormous proliferation of the number of diagrams and the amount of algebraic calculation is observed, requiring the development of programs which implement the diagrammatic expansion, and translate the resulting diagrams into input files for other programs which in turn are suited for the algebraic evaluation of individual diagrams. One example for such a "superprogram" is `GEFICOM` [29] which uses `QGRAF` [30] for the generation of diagrams, `LMP` [11] or `EXP` [31] for the diagrammatic expansion through the hard mass or large momentum procedure, and `MATAD` [32] and `MINCER` [33] for the evaluation of diagrams. Even nested expansions with a hierarchy of several scales are possible in this framework. (A more detailed description of the status of algebraic programs can be found in [6].) After performing the expansion in m^2/q^2 up to a given power, one may directly take the absorptive part and thus predict $\Pi(q^2)$ in the high energy region. The comparison with the Padé result (discussed in chapter 2) shows excellent agreement in the region of x between zero and 0.7 and thus down to fairly low energies (Fig. 7).

One may even suspect that, given sufficiently many terms of the absorptive part alone, an approximation of arbitrary precision can be achieved. This is indeed true for the two-loop result and the "double bubble" contribution with massless quarks in the internal loop, which are available in analytical form and thus can be used as "toy models". However, in both examples, the only threshold is located at $\sqrt{s} = 2m$ and convergence down to this point is

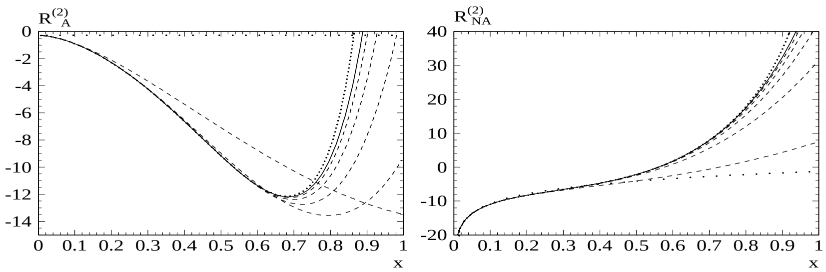

Figure 7: The Abelian contribution $R_A^{(2)}$ and the non-Abelian piece $R_{NA}^{(2)}$. Wide dots: no mass terms; dashed lines: including successively more mass terms $(m^2/s)^n$ up to $n = 5$; solid line: including mass terms up to $(m^2/s)^6$; narrow dots: semi-analytical result. The scale $\mu^2 = m^2$ has been adopted. (From [34].)

naturally expected. In contrast, the other diagrams have four-particle cuts at $\sqrt{s} = 4m$, suggesting convergence only above this point. This has been confirmed by a detailed study [34] of the double bubble contribution with equal masses in both fermion loops, where inclusion of an increasing number of terms does not lead to an improvement beyond $x \approx 0.5$. Given both real and imaginary parts, this problem could be and has been circumvented as discussed in chapter 2. However, below we will be interested in the situation where the absorptive piece only is available.

Nevertheless, the relative smallness of the four-particle contribution and the slow opening of the phase space reduce this effect and a fairly good approximation of R_A and R_{NA} is achieved even for $x = 0.7$, thus covering most of the interesting energy range (cf. Table 1). The same technique has also been used for the axial, the scalar and the pseudoscalar current [28,35]. (This motivates the step to $\alpha_s^3 m^4$ in chapter 4.) The agreement of the two-loop result described in chapter 2 with the threshold and the large momentum expansion in the respective ranges of validity demonstrate that the perturbative NLO prediction of $R(s)$ for massive quarks is under full control.

4 Quartic Mass Terms in NNLO form Operator Product Expansion

Fig. 7 suggests that the first three terms provide an excellent approximation at $x = 0.5$ and are quite acceptable even at $x = 0.7$. Using this line of reasoning, a possible route for a NNLO prediction (order α_s^3) of $R(s)$, including quark mass effects, is at hand. The massless result [8] and the m^2/s terms [9] have been obtained a long time ago. The strategy used in [10] allowed to predict the $\alpha_s^2 m^4/s^2$ terms in $R(s)$ by evaluating two-loop (!) tadpoles and massless propagators only. Additional ingredients are the operator product expansion and the renormalization group equations, plus certain anomalous dimensions. Using this method and algebraic programs it is thus possible to obtain the $\alpha_s^3 m^4/s^2$ terms from three-loop tadpoles and massless propagators [11,36]. Let me briefly describe this method: In a first step the OPE is applied to the time ordered product of two currents

$$\int \mathrm{d}x e^{iqx} T\big(j_\mu(x) j_\nu(0)\big) = (q_\mu q_\nu - g_{\mu\nu} q^2)\Big\{ A(q^2,\mu^2,\alpha_s)\mathbf{1} + B(q^2,\mu^2,\alpha_s)\frac{\bar{m}^2}{q^2}(\mu^2) + \sum_{n=1}^{6} \frac{1}{q^4} C_n(q^2,\mu^2,\alpha_s)\mathcal{O}_n \Big\}. \tag{13}$$

Only three of the six operators $\mathcal{O}_n$ with dimension four are gauge invariant and contribute to physical matrix elements:

$$\mathcal{O}_1 = G^2, \qquad \mathcal{O}_2 = m\bar{q}q, \qquad \mathcal{O}_6 = \bar{m}^4(\mu^2)\,, \tag{14}$$

the others are required for the proper construction to the coefficient functions C_n. For the NNLO calculation, C_1, C_2 and C_6 are required up to $\mathcal{O}(\alpha_s^2)$, $\mathcal{O}(\alpha_s^3)$ and $\mathcal{O}(\alpha_s^2)$ respectively. To obtain these coefficient functions, only massless propagator type integrals, at most of three loop, are needed. To calculate the vacuum matrix elements of $\mathcal{O}_1$ and $\mathcal{O}_2$, massive tadpole integrals – at most of three loop – are needed. In a last step one uses renormalization group invariance of the dimension four part of Eq. (13). Employing the anomalous dimension matrix [37] of $\mathcal{O}_{1,2,6}$ one finally obtains the coefficients of the terms $\alpha_s^3 \bar{m}^4 \ln^n q^2/\mu^2$ with $n = 1,2,3$. Only these terms contribute to the absorptive part and one finally arrives at [8,9,11,36]

$$R^v(s) = 3\Big\{ 1 - 6\,x^2 + \frac{\alpha_s}{\pi}\Big[1 + 12\,x - 22\,x^2\Big] + \Big(\frac{\alpha_s}{\pi}\Big)^2 \Big[1.40923 + 104.833\,x + x^2\,(139.014 - 4.83333\,l_x)\Big] + \Big(\frac{\alpha_s}{\pi}\Big)^3 \Big[-12.7671 + 541.753\,x + x^2\,(3523.81 - 158.311\,l_x + 9.66667\,l_x^2)\Big]\Big\}\,, \tag{15}$$

with $x \equiv \bar{m}^2(s)/s$, $l_x \equiv \ln(\bar{m}^2(s)/s)$ and $n_f = 5$.

5 Expansion techniques and electroweak interactions

Electroweak observables are frequently affected by the interplay between strong and electroweak interactions. Important examples are the hadronic contributions to the running of the QED coupling from the Thompson limit to M_Z, QCD effects on the ρ parameter and related quantities, and “mixed” vertex corrections affecting for example the Z decay rate. Quark mass effects and their perturbative treatment are important for $\alpha_{\mathrm{QED}}(M_Z)$. A detailed discussion of the last topic is beyond the scope of this paper and can be found in[15,38]. Let us present some aspects of the two remaining items.

Gauge boson self-energies, the mass of the top quark and QCD: The indirect determination of the top quark through quantum corrections prior to its observation in hadronic collisions can be considered one of the triumphs of the Standard Model. The experimental precision of the key observables, the masses of the top quark and the W boson together with the weak mixing angle as determined by asymmetry measurements has increased during the past years and this process will continue in the foreseeable future. In order to control the influence of the top quark at an adequate level the inclusion of QCD corrections in the top and bottom induced self energies is mandatory. The dominant terms are characterized by the ρ parameter which, in lowest order, is given by [39]

$$\Delta\rho = 3\sqrt{2}\frac{G_F m_t^2}{16\pi^2}. \tag{16}$$

In view of the large difference between pole and running mass at scale m_t

$$m_t(pole) = \bar{m}_t(m_t)\left(1 + \frac{4}{3}\frac{\alpha_s}{\pi} + \cdots\right) \tag{17}$$

inclusion of two and even three-loop QCD corrections to $\Delta\rho$ is mandatory.

Analytic results are available in two-loop approximation not only for the leading term [40] in $\Delta\rho$ but also for all self energies, with arbitrary top and bottom masses [41]. The resulting shift in the prediction for M_W for fixed G_F, α_{QED}, M_Z and $m_t = 175$ GeV amounts to 68 MeV, well comparable to the present precision and significantly larger than the anticipated accuracy of roughly 30 MeV. To arrive at a precise prediction for the central value and to control the theoretical uncertainty, three-loop QCD contributions to $\Delta\rho$ as well as to Δr are required. The ρ parameter [42] can again be expressed through diagrams with vanishing external momentum (vacuum or tadpole diagrams), the remaining quantities involve two point functions at non-vanishing external momentum and can be obtained[43] through an expansion in the small mass ratio M_Z^2/m_t^2. The leading three-loop term corresponds to a shift of -10.9 MeV. The first three terms, amounting to -13.7 MeV, are adequate for a prediction with an accuracy better than 1 MeV (Table 2). Conversely, this combined shift is equivalent to a reduction of the effective top mass by about 1.6 GeV.

δM_W in MeV	α_s^0	α_s^1	α_s^2
M_t^2	611.9	-61.3	-10.9
const.	136.6	-6.0	-2.6
$1/M_t^2$	-9.0	-1.0	-0.2

Table 2: The change in M_W separated according to powers in α_s and M_t in the on-shell scheme. (From [43].)

To exploit the precision expected from a future linear collider which will pin down m_t to better than 200 or perhaps even 100 MeV, the inclusion of α_s^2 terms is evidently mandatory.

Similar considerations[43] are valid for the effective weak mixing angle which can be deduced from the left right asymmetry or the forward backward asymmetry in a straightforward way.

An important issue in this connection is the size of uncertainties, arising either from uncalculated higher orders, or from the "parametric" uncertainties in α_s and m_t. Shifts of $\delta\alpha_s = 0.003$ and $\delta m_t = 5$ GeV lead to changes in M_W of -2.4 MeV and 35 MeV respectively. The uncertainty from uncalculated higher orders is completely negligible. A W-mass determination with a precision in the 10 MeV range should therefore be accompanied by a top mass measurement with a precision around or better than 1 GeV.

Mixed QCD and electroweak vertex corrections: As stated above, gauge boson self energies, in particular those induced by fermion loops, give rise to the dominant radiative corrections for electroweak precision observables. Nevertheless, for a complete treatment of $\mathcal{O}(\alpha\alpha_s)$ the inclusion of irreducible vertex corrections is necessary. These have to be distinguished from the reducible ones which are easily incorporated, if the electroweak result, including one-loop weak terms, is simply multiplied by the QCD correction factor $(1+\alpha_s/\pi+\cdots)$.

The physics and the techniques of calculation are markedly different for vertices leading to light (u, d, s and c) quark pairs on one hand [44] and for decays into $b\bar{b}$ on the other hand [45], a consequence of the presence of top quarks with their enhanced contribution to the vertex proportional m_t^2/M_W^2. The irreducible one-loop vertex diagrams are shown in Fig. 8.

To obtain all one-particle irreducible vertex diagrams in two-loop approximation , these have to be dressed with gluons in all conceivable ways. The resulting amplitudes are first studied for arbitrary q^2 by considering expansions in the ratio $x_Z = q^2/M_Z^2$ and $x_W = q^2/m_W^2$ (or for some diagrams, in $1/x_{Z,W}$). Even for the limiting values $x_Z = 1$ and $x_W = M_Z^2/M_W^2$ the exact results are well approximated, once sufficiently many terms are included. Us-

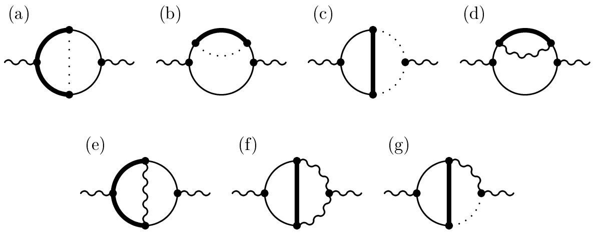

Figure 8: Diagrams contributing to $\delta\Gamma_b^W$ in $\mathcal{O}(\alpha)$. Thin lines correspond to bottom quarks, thick lines to top quarks, dotted lines to Goldstone bosons and inner wavy lines represent W bosons.

ing $\alpha_s = 0.12$, $\alpha = 1/129$, $\sin\theta_W = 0.223$ $M_Z = 91.19$ GeV, it is found[44] that the net effect of the nonfactorizable corrections is

$$\Gamma^{(\text{2-loop EW/QCD})} - \frac{\alpha_s}{\pi}\Gamma^{(\text{1-loop EW})}$$
$$= \begin{cases} -1.13(4) \times 10^{-4}\ \text{GeV} & \text{for } Z \to \bar{u}u \\ -1.60(6) \times 10^{-4}\ \text{GeV} & \text{for } Z \to \bar{d}d \end{cases} \tag{18}$$

The total change in the partial width $\Gamma(Z \to hadrons)$ is obtained by summing over 2 down-type and 2 up-type quarks:

$$\Delta\Gamma(Z \to u, d, s, c) = -0.55(3)\ \text{MeV} \tag{19}$$

which translates into the change of the strong coupling constant determined at LEP 1 equal to

$$\Delta\alpha_s = -\pi\frac{\Delta\Gamma(Z \to hadrons)}{\Gamma(Z \to hadrons)} = \pi\frac{0.55}{1741} \approx 0.001 \tag{20}$$

This shift is somewhat smaller but still of the same order of magnitude as the experimental accuracy and should to be taken into account in the final analysis of LEP 1 data. Electroweak parameters extracted from Z decays are not affected by this correction.

The two-loop corrections to the $Zb\bar{b}$ vertex are dominated by terms quadratic in m_t. The QCD corrections to these have been evaluated already some time ago[45]. The sub-leading terms $\propto \ln m_t^2$ were obtained in[46] and are of comparable magnitude, thus indicating relatively slow convergence of the series. The complete evaluation is thus mandatory and has been recently been performed[47]. In contrast to the previous case one is confronted with three different scales, the masses of top, the W and the Z boson.

Using the hard mass procedure for $m_t^2 \gg M_Z^2, M_W^2$, one may factor out the m_t–dependence. However, for a part of the diagrams one still is left with two-scale and even three-scale integrals involving M_Z^2 and M_W^2 and $\xi_W M_W^2$, where ξ_W is the electroweak gauge parameter which has been kept in [47]. Although they appear to be only one-loop integrals, their exact evaluation up to $\mathcal{O}(\epsilon)$ is inconvenient. Instead, the results [47] were obtained by applying the hard mass procedure to these kinds of diagrams once more, this time using $\xi_W M_W^2, M_W^2 \gg M_Z^2$. This seemingly unrealistic choice of scales can be well justified: It is not possible for an expansion to distinguish the inequality $M_W^2 \gg M_Z^2$ from $4M_W^2 \gg M_Z^2$ or $(m_t + M_W)^2 \gg M_Z^2$, the latter ones being perfectly alright. The only matter is to perform the expansion on the appropriate side of all thresholds, and here one is concerned with thresholds at $2M_W$ and at $m_t + M_W$. Therefore, the choice $M_W^2 \gg M_Z^2$ is to be understood purely in this technical sense. Graphically this continued expansion looks as follows:

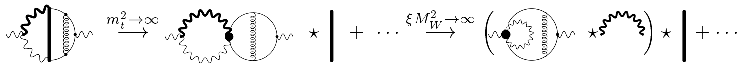

where only those terms are displayed which are relevant in the discussion above and all others contributing to the hard mass procedure are merged into the ellipse. The thick plain line is the top quark, the thick wavy one a Goldstone boson with mass squared $\xi_W M_W^2$, for example. The thin plain lines are b–quarks, the inner thin wavy lines are W–bosons, the outer ones Z-bosons. The spring-line is a gluon. The mass hierarchy is assumed to be $m_t^2 \gg \xi_W M_W^2 \gg M_W^2 \gg M_Z^2$. The freedom in choosing the magnitude of ξ_W provides a welcome check of the routines and the results.

The outcome of this procedure is a nested series: The coefficients of the M_W/m_t–expansion are in turn series in M_Z/M_W. Note that in contrast to the decay into u, d, s, c there is no threshold at M_W which makes an additional expansion in M_W/M_Z unnecessary.

In view of this calculation the procedure of successive application of the hard mass procedure resp. the large momentum procedure has been implemented in a Fortran 90 program named `EXP` [31]. Therefore, given an arbitrary hierarchy of mass scales, the computation of a three-loop two-point function can now be done fully automatically. Even more, the link to the Feynman diagram generator `QGRAF` [30] in a common environment called `GEFICOM` [29] allows to obtain the result of a whole physical process without any human interference except for specification of the process and final renormalization.

Finally, the result for the W–induced corrections to the Z–decay rate $\delta\Gamma^W(Z \to b\bar{b})$ is conveniently presented in the form of the renormalization scheme independent difference to the decay rate into $d\bar{d}$. Inserting the on-shell top mass $m_t = 175$ GeV, the Z–mass $M_Z = 91.19$ GeV and $\sin^2\theta_W = 0.223$ gives [47]

$$
\begin{aligned}
&\delta\Gamma^W(Z\to b\bar{b}) - \delta\Gamma^W(Z\to d\bar{d}) = \Gamma^0 \frac{1}{\sin^2\theta_W}\frac{\alpha}{\pi}\Bigg\{ -0.50 + (0.71-0.48) \\
&+ (0.08-0.29) + (-0.01-0.07) + (-0.007-0.006) + \frac{\alpha_s}{\pi}\Bigg[1.16 + (1.21 \\
&-0.49) + (0.30-0.65) + (0.02-0.21+0.01) + (-0.01-0.04+0.004)\Bigg]\Bigg\} \\
&= \Gamma^0 \frac{1}{\sin^2\theta_W}\frac{\alpha}{\pi}\Bigg\{ -0.50 - 0.07 + \frac{\alpha_s}{\pi}\Bigg[1.16+0.13\Bigg]\Bigg\}\,, \qquad (21)
\end{aligned}
$$

where the factor $\Gamma^0\alpha/(\pi\sin^2\theta_W)$ with $\Gamma^0 = M_Z\alpha/(4\sin^2\theta_W\cos^2\theta_W)$ has been pulled out for convenience. The numbers after the first equality sign correspond to successively increasing orders in $1/m_t^2$, where the brackets collect the corresponding constant, $\log m_t$ and, if present, $\log^2 m_t$–terms. The numbers after the second equality sign represent the leading m_t^2–term and the sum of the sub-leading ones. The $\mathcal{O}(\alpha)$ and $\mathcal{O}(\alpha\alpha_s)$–results are displayed separately. Comparison of this expansion of the one-loop terms to the exact result [48] shows agreement up to 0.01% which gives quite some confidence in the $\alpha\alpha_s$–contribution. One can see that although the m_t^2–, m_t^0– and $m_t^0\log m_t$–terms are of the same order of magnitude, the final result is surprisingly well represented by the m_t^2–term, since the sub-leading terms largely cancel among each other.

The uncertainty from uncalculated higher order QCD terms is far below the foreseeable experimental precision, and the parametric uncertainty from α_s and m_t dominates. An important lesson to be learned from the $Zb\bar{b}$ vertex in one- and two-loop approximation concerns the interplay between “dominant” and “sub-leading” pieces: whenever leading and sub-leading terms are of comparable magnitude, inclusion of a sizeable number of terms in the expansion is required. The estimate of the final result or of theoretical uncertainties based on the first two terms of the series may lead to a wrong or misleading result.

6 Summary

Expansion techniques for Feynman amplitudes combined with sophisticated computer algebra programs have lead to remarkable progress in multiloop calculations during the past years. Problems with different mass and energy scales can be treated with nested series. Powerful computers allow to evaluate many terms in these expansions, and smallness of the expansion parameter is thus no longer required. These techniques have been successfully applied to purely hadronic as well as to electroweak observables.

Acknowledgments: I would like to thank Joan Sola for organizing this pleasant and very successful conference. The material presented in this review has been developed in enjoyable and fruitful collaborations with K. Chetyrkin, A. Czarnecki, R. Harlander, Th. Seidensticker and M. Steinhauser. The paper would never have been completed without the TEXnical help of R. Harlander. Work supported by *DFG-Forschergruppe "Quantenfeldtheorie, Computeralgebra und Monte-Carlo-Simulationen"* (DFG Contract KU 502/6-1) and BMBF Contract 056 KA 93 P6 at the University of Karlsruhe.

1. K.G. Chetyrkin, S.G. Gorishny and F.V. Tkachov, *Phys. Lett.* **B 119** (1982) 407; F.V. Tkachov, *Phys. Lett.* **B 124** (1983) 212; S.G. Gorishny, S.A. Larin, and F.V. Tkachov, *Phys. Lett.* **B 124** (1983) 217; K.G. Chetyrkin, *Phys. Lett.* **B 126** (1983) 371; G.B. Pivovarov and F.V. Tkachov, Rep. No. INR P-0370 (Moscow, 1984); K.G. Chetyrkin and V.A. Smirnov, Rep. No. INR P-518 (Moscow, 1987); S.G. Gorishny and S.A. Larin, *Nucl. Phys.* **B 283** (1987) 452; K.G. Chetyrkin, *Theor. Math. Phys.***75** (1988) 346, *Theor. Math. Phys.***76** (1988) 809; V.A. Smirnov, *Mod. Phys. Lett.* **A 3** (381) 1988; S.G. Gorishny, *Nucl. Phys.* **B 319** (1989) 633; V.A. Smirnov, *Comm. Math. Phys.* **134** (1990) 109; K.G. Chetyrkin, Rep. No. MPI-PAE/PhT 13/91 (Munich, 1991); F.V. Tkachov, *Int. J. Mod. Phys.* **A 8** (1993) 2047; G.B. Pivovarov and F.V. Tkachov, *Int. J. Mod. Phys.* **A 8** (1993) 2241.
2. For reviews of the expansion methods and their applications see: V.A. Smirnov, *Mod. Phys. Lett.* **A 21** (1485) 1995; V.A. Smirnov, *Renormalization and Asymptotic Expansion* (Birkhäuser, Basel, 1991); K.G. Chetyrkin, J.H. Kühn and A. Kwiatkowski, *Phys. Reports* **277** (189) 1966; J. Fleischer, A.V. Kotikov and O.L. Veretin, Acta Phys. Polon. **B 29** (1998) 2611.
3. M. Beneke and V.A. Smirnov, *Nucl. Phys.* **B 522** (1998) 321.
4. A. Czarnecki and K. Melnikov, *Phys. Rev. Lett.* **80** (1998) 2531.
5. M. Beneke, A. Signer, and V.A. Smirnov, *Phys. Rev. Lett.* **80** (1998) 2535.
6. R. Harlander and M. Steinhauser, *Automatic Computation of Feynman Diagrams*, Rep. Nos. TTP98-41, BUTP-98/28, hep-ph/9812357, to be published in *Progr. Part. Nucl. Phys.*, Vol. 43.
7. K.G. Chetyrkin, A.L. Kataev, and F.V. Tkachov, *Phys. Lett.* **B 85** (1979) 277; M. Dine and J. Sapirstein, *Phys. Rev. Lett.* **43** (1979) 668; W. Celmaster and R.J. Gonsalves, *Phys. Rev. Lett.* **44** (1980) 560.

8. S.G. Gorishny, A.L. Kataev, and S.A. Larin, *Phys. Lett.* **B 259** (1991) 144; L.R. Surguladze and M.A. Samuel, *Phys. Rev. Lett.* **66** (1991) 560; (E) ibid., 2416; K.G. Chetyrkin, *Phys. Lett.* **B 391** (1997) 402.
9. K.G. Chetyrkin and J.H. Kühn, *Phys. Lett.* **B 248** (1990) 359.
10. K.G. Chetyrkin and J.H. Kühn, *Nucl. Phys.* **B 432** (1994) 337.
11. R. Harlander, *Quarkmasseneffekte in der Quantenchromodynamik und asymptotische Entwicklung von Feynman-Integralen*, Shaker Verlag, Aachen 1998, ISBN 3-8265-4545-1.
12. G. Källén and A. Sabry, K. Dan. Vidensk. Selsk. Mat.-Fys. Medd. **29** (1955) No. 17, see also J. Schwinger, Particles, *Sources and Fields*, Vol.II, (Addison-Wesley, New York, 1973).
13. K.G. Chetyrkin, J.H. Kühn, and M. Steinhauser, *Phys. Lett.* **B 371** (1996) 93; *Nucl. Phys.* **B 482** (1996) 213; *Nucl. Phys.* **B 505** (1997) 40.
14. A.H. Hoang, J.H. Kühn, and T. Teubner, *Nucl. Phys.* **B 452** (1995) 173.
15. K.G. Chetyrkin, A.H. Hoang, J.H. Kühn, M. Steinhauser, and T. Teubner, *Eur. Phys. J.* **C 2** (1998) 137.
16. S.G. Gorishny, A.L. Kataev, and S.A. Larin, *Nuovo Cim.* **92A** (1986) 119.
17. R. Barbieri, R. Gatto, R. Kögerler and Z. Kunszt, *Phys. Lett.* **B 57** (1975) 455; B.H. Smith and M.B. Voloshin, *Phys. Lett.* **B 324** (1994) 17.
18. W. Fischler, *Nucl. Phys.* **B 129** (1977) 157; A. Billoire, *Phys. Lett.* **B 92** (1980) 343.
19. J.A.M. Vermaseren, *Symbolic Manipulation with FORM*, (Computer Algebra Netherlands, Amsterdam, 1991).
20. F.V. Tkachov, *Phys. Lett.* **B 100** (1981) 65; K.G. Chetyrkin and F.V. Tkachov, *Nucl. Phys.* **B 192** (1981) 159.
21. D.J. Broadhurst, *Z. Phys.* **C 54** (1992) 599.
22. J. Fleischer and O.V. Tarasov, *Z. Phys.* **C 64** (1994) 413.
23. D.J. Broadhurst, J. Fleischer, and O.V. Tarasov, *Z. Phys.* **C 60** (1993) 287.
24. P.A. Baikov and D.J. Broadhurst, *4th International Workshop on Software Engineering and Artificial Intelligence for High Energy and Nuclear Physics (AIHENP95)*, Pisa, Italy, 3-8 April 1995. Published in Pisa AIHENP (1995) 167.
25. K.G. Chetyrkin, R. Harlander, and M. Steinhauser, *Phys. Rev.* **D 58** (1998) 014012.
26. A.H. Hoang, *Phys. Rev.* **D 56** (1997) 7276.
27. K.G. Chetyrkin, J.H. Kühn, and M. Steinhauser, *Nucl. Phys.* **B 505**

(1997) 40.
28. R. Harlander and M. Steinhauser, *Phys. Rev.* **D 56** (1997) 3980.
29. K.G. Chetyrkin and M. Steinhauser, unpublished.
30. P. Nogueira, *J. Comp. Phys.* **105** (1993) 279.
31. Th. Seidensticker, Diploma thesis (University of Karlsruhe, 1998), unpublished.
32. M. Steinhauser, *Drei-Schleifen-QCD-Korrekturen zu Zwei-Punkt-Funktionen*, Shaker Verlag, Aachen, 1996, ISBN 3-8265-1680-X.
33. S.A. Larin, F.V. Tkachov, and J.A.M. Vermaseren, Rep. No. NIKHEF-H/91-18 (Amsterdam, 1991).
34. K.G. Chetyrkin, R. Harlander, J.H. Kühn, and M. Steinhauser, *Nucl. Phys.* **B 503** (1997) 339.
35. R. Harlander and M. Steinhauser, *Eur. Phys. J.* **C 2** (1998) 151.
36. K.G. Chetyrkin, R. Harlander, and J.H. Kühn, in preparation.
37. V.P. Spiridonov and K.G. Chetyrkin, *Sov. J. Nucl. Phys.* **47** (1988) 522.
38. J.H. Kühn and M. Steinhauser, *Phys. Lett.* **B 437** (1998) 425.
39. M. Veltman, *Nucl. Phys.* **B 123** (1977) 89.
40. A. Djouadi and C. Verzegnassi, *Phys. Lett.* **B 195** (1987) 265; A. Djouadi, *Nuovo Cim.* **100A** (1988) 357.
41. B.A. Kniehl, *Nucl. Phys.* **B 347** (1990) 65; B.A. Kniehl, J.H. Kühn, and R.G. Stuart, *Phys. Lett.* **B 214** (1988) 621.
42. L. Avdeev, J. Fleischer, S. Mikhailov and O. Tarasov, *Phys. Lett.* **B 336** (1994) 560; (E) ibid. **B 349** (1995) 597; K.G. Chetyrkin, M. Steinhauser and J.H. Kühn, *Phys. Lett.* **B 351** (1995) 331.
43. K.G. Chetyrkin, M. Steinhauser and J.H. Kühn, *Phys. Rev. Lett.* **75** (1995) 3394.
44. A. Czarnecki and J.H. Kühn, *Phys. Rev. Lett.* **77** (1996) 3955; (E) ibid. **80** (1998) 893.
45. J. Fleischer, F. Jegerlehner, P. Rączka and O.V. Tarasov, *Phys. Lett.* **B 293** (1992) 437; G. Buchalla and A. Buras, *Nucl. Phys.* **B 398** (1993) 285; G. Degrassi, *Nucl. Phys.* **B 407** (1993) 271; K.G. Chetyrkin, A. Kwiatkowski and M. Steinhauser, *Mod. Phys. Lett.* **A 8** (1993) 2785.
46. A. Kwiatkowski and M. Steinhauser, *Phys. Lett.* **B 344** (1995) 359.
47. R. Harlander, T. Seidensticker, and M. Steinhauser, *Phys. Lett.* **B 426** (1998) 125.
48. A. Akhundov, D. Bardin, and T. Riemann, *Nucl. Phys.* **B 276** (1986) 1; J. Bernabeu, A. Pich, and A. Santamaria, *Phys. Lett.* **B 200** (1988) 569; B.W. Lynn and R.G. Stuart, *Phys. Lett.* **B 252** (1990) 676.